Ultrasound Capsule Endoscopy With a Mechanically Scanning Micro-ultrasound

Qiu, Yongqiang; Huang, Yaocai; Zhang, Zhiqiang; Cox, Benjamin F.; Liu, Rong; Hong, Jiehan

Published in:
Ultrasound in Medicine and Biology

DOI:
10.1016/j.ultrasmedbio.2019.12.003

Publication date:
2020

Document Version
Peer reviewed version

Author Accepted Manuscript: Qiu, Yongqiang et al. "Ultrasound Capsule Endoscopy With a Mechanically Scanning Micro-ultrasound: A Porcine Study". Ultrasound in Medicine and Biology. 2020. https://doi.org/10.1016/j.ultrasmedbio.2019.12.003

Ultrasound capsule endoscopy with a mechanically scanning micro-ultrasound: a porcine study

Authors: Yongqiang Qiu[a,1,#], Yaocai Huang[b,#], Zhiqiang Zhang[b], Benjamin F. Cox[c], Rong Liu[b], Jiehan Hong[b], Peitian Mu[b], Holly S. Lay[a,2], Gerard Cummins[d], Marc P.Y. Desmulliez[d], Eddie Clutton[e], Hairong Zheng[b], Weibao Qiu[b*], Sandy Cochran[a]

a. School of Engineering, University of Glasgow, Glasgow, UK
b. Paul C. Lauterbur Research Center for Biomedical Imaging, Shenzhen Institutes of Advanced Technology, Chinese Academy of Sciences, Shenzhen, China
c. School of Medicine, University of Dundee, Dundee, UK
d. School of Engineering and Physical Sciences, Heriot-Watt University, Edinburgh, UK
e. Royal (Dick) School of Veterinary Studies, University of Edinburgh, UK
1. Faculty of Engineering and Technology, Liverpool John Moores University, Liverpool, UK
2. FUJIFILM VisualSonics, Inc., Toronto, Canada

# These authors contributed equally to this work.
*Corresponding author: Weibao Qiu, Email: wb.qiu@siat.ac.cn

Abstract

Wireless capsule endoscopy has been used for the clinical examination of the gastrointestinal (GI) tract for two decades. However, most commercially available devices only utilise optical imaging to examine the GI wall surface. Using this sensing modality, pathology within the GI wall cannot be detected. Microultrasound (µUS) using high-frequency (>20MHz) ultrasound can provide a means of transmural or cross-sectional image of the GI tract. Depth of imaging is approximately 10 mm with a resolution of between 40-120 µm that is sufficient to differentiate between subsurface histological layers of the various regions of the GI tract. Ultrasound capsule endoscopy (USCE) uses a capsule equipped with µUS transducers that are capable of imaging below the GI wall surface, offering thereby a complementary sensing technique to optical imaging capsule endoscopy. In this work, a USCE device integrated with a ~30 MHz ultrasonic transducer was developed to capture a full 360° image of the lumen. The performance of the device was initially evaluated using a wire phantom, indicating an axial resolution of 69.0 µm and lateral resolution of 262.5 µm. Later, *in vivo* imaging performance was characterised in the oesophagus and small intestine of anaesthetized pigs. The reconstructed images demonstrate clear layer differentiation of the lumen wall. The tissue thicknesses measured from the B-scan images show good agreement with ex vivo images from the literature. The high-resolution ultrasound images in the *in vivo* porcine model achieved with this device is an encouraging preliminary step in the translation of these devices towards future clinical use.

Keywords: Capsule endoscopy, high-frequency ultrasound, micro-ultrasound capsule endoscopy, *in vivo* porcine animal study.

INTRODUCTION

Conventional endoscopy assesses the gastrointestinal (GI) tract using a flexible probe equipped with either an optical imaging sensor (and a light source) or an ultrasound-emitting device (Dimagno et al. 1980; Valdastri et al. 2012). Acquired images of the internal GI structure assist in the diagnosis of numerous conditions. However, conventional endoscopy requires the use of highly trained staff, is uncomfortable for patients, sometimes necessitating the use of sedatives or even anaesthetics. Furthermore, it cannot readily investigate all parts of the GI tract, e.g., the small intestine (Cummins et al. 2019). Capsule endoscopy (CE) also integrates optical sensors within an easily-swallowed capsule form factor, typically 11 mm in diameter and 24 - 33 mm long; with a mass of 3 grams, that allows minimally invasive inspection of the entire GI tract for up to six hours, constrained by the battery life (Iddan et al. 2000; Moglia et al. 2009; Wang et al. 2013). These devices are capable of acquiring a considerable amount of image data of the GI tract, which assists in the diagnosis of a wide range of gastrointestinal disease. However, similar to conventional endoscopy, the assessment remains reliant on camera imaging. This limits diagnostic utility to superficially visible manifestations of diseases which are often late stage and difficult to interpret due to visual overlap (Hamilton 2012).

An alternative to optical endoscopy is ultrasound endoscopy (EUS), which is a routinely used clinical imaging modality for the examination of the oesophageal and stomach linings as well as the walls of the upper and lower GI tract. Conventional EUS typically employs ultrasound frequencies in the range 5–18 MHz, corresponding to axial resolutions of 0.2–0.8 mm and depths of 2–8 cm, respectively (McNally 2010). Lower frequency (5-20 MHz) imaging enables observation of organs located beyond the wall of the gastrointestinal tract whereas higher frequencies (>20 MHz) may provide more detailed images of the gut wall at the expense of lower depth penetration (Correia 2009; Wang et al. 2017a). High-frequency imaging is usually achieved through the insertion of high-resolution ultrasound, also known as micro-ultrasound, mini-probes into conventional endoscopes via the biopsy channel (Schembre et al. 2005).

These probes have improved axial and lateral image resolution relative to conventional EUS frequencies, and are capable of producing highly-detailed submucosal images that include information on the structure and tissue composition.

Following the example of clinical utility set by EUS, the inclusion of ultrasound imaging into capsule endoscopy is a desirable means of improving the diagnostic capabilities of CE (Cummins et al. 2019). Ultrasound capsule endoscopy (USCE) has been proposed by several groups (Correia 2009; Lay et al. 2019; Lee et al. 2014; Memon et al. 2015; Memon et al. 2016; Wang et al. 2017a). These efforts include the integration of ring arrays composed of multiple capacitive micromachined ultrasonic transducers (CMUTs) that operate with frequencies comparable to conventional endoscopy, providing a 360° image of the organs surrounding the GI tract (Memon et al. 2015; Memon et al. 2016; Wang et al. 2017a). An example of such a device is shown in Fig. 1. The development of micro-ultrasound capsule endoscopy (μUSCE) capable of producing 360° cross-sectional ultrasound B-scan images is of particular interest due to high-resolution images that can be achieved of the constituent layers of the GI tract (Panes et al. 2013). Cross-sectional (i.e. transmural) imaging allows assessment of disease extent across the GI wall. μUSCEs reported to date include a rotating mirror as shown in Fig. 1(a) (Iddan 2010), unfocused 10 MHz transducer (Lee et al. 2014), focused 30 MHz transducers (Lay et al. 2019), and proposed array-based methods as shown in Fig. 1(b) (Arneson et al. 2014; Lay et al. 2018). The rotational mirror solution arises complexity and difficulty in manufacture and assembly of the acoustic mirror. The array-based solution inherits the technical challenges in the manufacture of high frequency, miniaturized, circumferential transducer arrays. The rate of development of μUSCE technology has been slow due to the challenges associated with the integration and miniaturization required to realize these capsules.

However, mechanical scanning of the transducer can provide the clinician with a high-resolution, transmural 360° view of the tissue layers of the GI tract and is therefore of immediate interest as it can potentially provide highly detailed cross sectional images of the GI wall. Compared to the other two solutions, mechanical rotating transducer, Fig. 1(c), simplifies device fabrication and electronics and is

therefore particularly useful for USCE in its early development, paralleling to the development of the similar solution in intravascular ultrasound (Yu et al. 2017). In a previous study, we demonstrated a mechanically scanned ultrasound capsule, shown in Fig. 1(c), that showed potential for clinical applications based on experimental data from *ex vivo* tests (Wang et al. 2017b). The new capsule was characterized on the bench using wire phantoms. Successful *in vivo*, high-resolution ultrasound results are also reported for the cross-sectional imaging the small intestine and oesophagus of porcine animal models.

MATERIALS AND METHODS

Capsule Device

The structure of the proof of concept µUSCE device is shown in Fig. 1(d) and consists of a micromotor, a transducer holder and an ultrasound transducer encased in a biocompatible shell with an acoustically transparent window. The USCE shell of diameter 10 mm and length 30 mm was made from biocompatible poly (methyl methacrylate) PMMA, (Z=3.2 MRayl). This size agrees to the majority of video capsule endoscopes on the market, 11 mm in diameter and 24–33 mm in length (Stewart et al. 2017). The USCE is connected to external instrumentation that drives the motor and controls ultrasound transduction via a Teflon tube of outer diameter 1.7 mm and inner diameter 1.1 mm (Shenzhen Woer Heat-Shrinkable Material Co., Ltd. China). A tethered design was used at this stage to ease retrieval of the device during *in vivo* trials and provide control for the operation of the ultrasonic transducer and the motor due to the difficulty in sourcing a suitably sized commercially available integrated circuit (IC) that could be integrated inside the capsule. The rotation of the motor (TT Motor Shenzhen Industrial Co, Ltd, China) was controlled by varying the amplitude and direction of the input DC current. The motor rotated the transducer 360° in an oscillatory manner, alternately clockwise and counterclockwise in every 0.2 seconds with a ±1.2 V input. This leads to a frame rate of 5 fps for the system.

The µUS transducer was fabricated from a piezocrystal $LiNbO_3$ to operate at a resonant frequency ~30 MHz, with a press-focused focal distance of 8 mm and the diameter of 3 mm. Two matching layers were

designed for the transducer to compensate for acoustic impedance mismatch between tissue and piezoelectric material. The first matching layer (Z = 7.3 MRayl) with 14 μm thickness was made of Insulcast 501 and Insulcure 9 (American Safety Technologies, Roseland, NJ), and 2-3 μm silver particles (Sigma-Aldrich Inc., St. Louis, MO). The second layer was made by depositing an 18 μm thick Parylene C (Z = 2.5 MRayl) layer. E-solder 3022 (Von Roll Isola, New Haven, CT) with an acoustic impedance of 5.9 MRayl was used as the backing layer.

The transducer is placed in a PMMA holder that aligns it with both the central longitudinal axis of the capsule and the acoustic window. The distance from the front face of the transducer to the capsule outer surface was about 6 mm. During rotation, the transducer emits and receives ultrasound through an acoustic window in the capsule shell. The acoustic window is made from polydimethylsiloxane (PDMS) to minimize the reflection and attenuation during the ultrasound transmission. To further optimize the acoustic transmission, a layer of 18 μm thick Parylene C was coated on both surfaces of the PDMS material.

All components and bonding were achieved with medical-grade epoxy (Epoxy Technologies, Billerica, MA, USA). The final μUSCE device is shown in Fig. 2(a). The quality of the seal and the mechanical robustness of empty capsules were quantified prior to insertion into porcine animal models to verify safety.

Imaging Platform

An imaging platform was developed specifically for the evaluation of the proposed μUSCE device as shown in Fig. 2. A pair of metal-oxide-semiconductor field effect transistors (MOSFETs) (TC6320, Supertex Inc., Sunnyvale, CA) was employed for the pulse generation. The MOSFETs were excited by two drivers (EL7158, Intersil Corporation, Milpitas, CA), and a field programmable FPGA device (Cyclone-V 5CGXFC7D7F31C8N, Altera Corporation, San Jose, CA). The excitation pulses sent from the imaging platform are single cycle, 30MHz center frequency, and +/-60 V amplitude. In the data acquisition circuitry, a low-noise amplifier (AD8331, Analog Devices, Canton, MA) was used to amplify

the echo signals. The gain was set to 45 dB during the data acquisition process. An analog filter was designed for anti-aliasing filtering to remove high-frequency noise. A 12-bit ADC (AD9230, Analog Devices) with a maximal sampling rate of 250 mega-samples per second (MSPS), was employed to digitize the echoic signals. The ultrasound data was then transferred to a computer via a USB 3.0 interface (CYUSB3014, Cypress, San Jose, CA). The data acquisition process was described in detail previously by our group (Wang et al. 2017b), the process diagram is shown in Fig. 2(c).

The control of the motor back and forth rotation was realized through two analog switch channels to control the supply of positive and negative power inputs. The circuit diagram and control time sequences of the positive and negative power paths and relay path are shown in Fig. 3.

Animal Study

To demonstrate the effectiveness of the device, *in vivo* studies were performed in the oesophagus and small intestine of two anaesthetised female Landrace pigs. This model was chosen because of the anatomical and physiological similarities between the GI tract of pigs and humans (Kararli 1995; Swindle et al. 2012; Ziegler et al. 2016). The experiments were conducted after approval by the Animal Welfare and Ethical Review Board of the Roslin Institute (Roslin, Midlothian, EH25 9RG) and under UK Home License (Project Licence: P3F417A41) in accordance with the Animal (Scientific Procedures) Act 1986.

Two four-month old female Landrace pigs weighing 48 and 51 kg were used in the studies. Food was withheld for 12 hours before anaesthesia to obtain a relatively empty proximal intestine and access to water was maintained until the pre-anaesthetic medication was injected intramuscularly. This medication was midazolam (0.5 mg kg^{-1}), ketamine (5 mg kg^{-1}) and medetomidine (2.5 µg kg^{-1}). As with previous work (Lay et al. 2019), anaesthesia was induced with isoflurane (IsoFlo, Zoetis, Surrey, UK) vaporized in oxygen and nitrous oxide administered via a Bain breathing system and facemask. A cannula was placed in the auricular vein and after intravenous propofol, the trachea was intubated. Anaesthesia was maintained with isoflurane delivered in an oxygen/air mixture via a circle breathing system. Ringer's lactate solution (Aqupharm No 11, Animalcare, York, UK) was administered at 10 ml kg^{-1} hr^{-1} throughout

each study to maintain fluid and electrolyte levels. During anaesthesia, the lungs of the pigs were mechanically ventilated to maintain normocapnia and vital signs were monitored throughout the experiment by veterinary anaesthetists.

Two capsule prototypes were created and each was tested in both the oesophagus and small intestine of the anesthetised pigs where ultrasonic echoes were collected during experiments. Because of the constrained shared space with anaesthetic intubation, a shortened, wide-diameter endotracheal tube was inserted transorally into the oesophagus. This allowed rapid, direct access to the proximal oesophagus. During the study, the capsule was inserted at least 36 cm beyond the mouth as measured by the length of tether inserted down the endotracheal tube. Image data from the capsule was collected at three different positions, separated from each other by 2 cm as measured from the length of tether manually pulled from the oesophagus. An artificial stoma was surgically created on the pig's lateral side to directly access the small intestine. The capsule was inserted directly into the small intestine through the artificial stoma with the pig lying on the other side under general anaesthetic. Three different points were imaged in the small intestine and were measured to be 60 cm, 40 cm and 20 cm from the entrance of the stoma as measured by the length of tether manually pulled from the stoma. The capsule was fixed at these points during imaging through the use of surgical tape that attached the tether to the surrounding skin. The distances were marked with tape before the experiments. A saline drip (1-2 drips/s) applied to the entrance of the stoma and oesophagus ensured lubricity to facilitate capsule insertion and acoustic coupling between the capsule and the surrounding tissue.

RESULTS

Characterisation of μUSCE

The pulse-echo response of the transducer was measured to characterise its performance. It was mounted on a holder and immersed in a tank filled with deionized water. A glass reflector was placed a distance of 8 mm from the transducer, corresponding with its focal length. The centre frequency of the

ultrasound transducer was measured from the pulse-echo waveform to be 28.15 MHz and the −6 dB bandwidth is about 50.1%.

The spatial resolution of the USCE was characterized using a wire phantom consisting of five 25 μm diameter tungsten wires (Advent Research Materials Ltd, Oxford, UK) spaced 1.4 mm apart. These wires were placed close to the focal point of the transducer in the capsule and the radial distances of all 5 wires to the capsule shell were in a range of 1.5-2.5 mm. Fig. 4(a) shows the wire phantom image acquired using the proposed μUSCE device with a dynamic range of 50 dB. The −6 dB (FWHM, full-width half-maximum) axial and lateral resolutions of the μUSCE device were 69.0 μm and 262.5 μm, respectively.

Small Intestine Imaging

B-scan data of the small intestine was successfully recorded during the *in vivo* experiments. An example of a post-processed B-scan image of the small intestine, which is reconstructed from 797 sets of A-scan data, is shown in Fig. 5, demonstrating clear layer differentiation of the lumen wall structure.

The sublayers of the small intestine, i.e. mucosa, submucosa, muscularis propria and serosa, can be clearly observed from the B-scan image (Fig. 5). The tissue sublayer thicknesses represented in the B-scan image correlates with hematoxylin and eosin (H&E) slides and *ex vivo* ultrasound images of the porcine small intestine from the literature (Cox et al. 2017). During the experiment, the small intestine tissue tended to envelop and compress itself against the capsule shell. Hence, the ring down artifact caused by the capsule shell reduced the visibility of the mucosa layer and varied the sublayer thickness.

Oesophagus Imaging

B-scan data of the oesophagus was successfully recorded during the *in vivo* experiments. An example of a post-processed image, which is reconstructed from 876 sets of A-scan data, is shown in Fig. 6. Physiologically, the natural corrugations of the tissue of an empty oesophagus form longitudinal folds; some of these folds flatten out and compress the capsule during the passage. This can be directly observed from Fig. 6: clear layer differentiation can be seen at the bottom-left of the image where the tissue folded

away from the capsule, while ring down artifacts shows at the top-right of the image led to poor layer differentiation except for the deep layer (i.e. Adventitia). Moreover, pure ring down artifact can be noticed at the bottom-right of the image. This is thought to be caused by air and poor acoustic coupling between the capsule and the tissue. More interestingly, an oval-shaped feature can be noticed at the right of the image, which is thought to be a vein or lymph node, as the size and imaging characteristics corresponding to relevant anatomical literature (Saar 1962).

DISCUSSION AND CONCLUSIONS

Capsule endoscopy has revolutionized the endoscopic imaging through miniaturization, enabling examination of the entire length of the GI tract with minimal discomfort to patients. However, most commercially available capsule devices still use white light imaging to image the GI tract, limiting diagnosis to just surface examination. Some advanced capsules have been proposed for non-optical diagnostic biomarkers (Cummins et al. 2019) and therapeutic applications (Stewart et al. 2017).

Therefore, this study investigated the optimisation of the scan method and further evaluated the device with *in vivo* animal tests. This paper expands on this earlier work (Wang et al. 2017b) on two fronts: (1) by describing the next generation of this technology and (2) by reporting on the tests of our capsule in anaesthetised pigs and achievement of *in vivo* high-resolution ultrasound images. On the technological side, a simpler mechanical setup and control method was used to achieve 360° sectional images via mechanical scanning of a high frequency (~30 MHz) ultrasound transducer. This overcomes the manufacture challenges on 3D printing of small parts, e.g. small gears, and improve the reliability of the device. It demonstrated that micro-ultrasound with a mechanical rotation scheme is feasible for assessing the GI tract by providing high-resolution ultrasound images. The proposed scheme in this study paves the way for the implementation of capsule ultrasound devices. This is further demonstrated by the high-resolution, cross-sectional *in vivo* imaging of the small intestine and oesophagus possible with this capsule.

The 10 mm diameter and 30 mm length of the prototype devices conformed to commercial video capsule endoscopes (VCE) dimensions, which are found to be acceptable for clinical use. It is possible to short the length but require more engineering work. The motor can be customized for at least 4mm shorter than current design. Although wireless capsules are desirable for the inspection of full GI tract, the tethered devices not only allow the research on the ultrasound imaging modality in the capsule form to be successful after insulating other challenges in the development of CE devices, such as power supply, data communication, location tracking and locomotion control (Basar et al. 2012; Ciuti et al. 2016), but also give extra benefits in the development stage by its capability of pull-back to the marked positions for repeated tests. Moreover, there is no easily suitable, commercially-available ICs for USCE onboard image processing.

Satisfactory acoustic coupling between the capsule and the mucosa of the lumen wall was achieved augmented by saline drips during the *in vivo* experiments. Good agreement of layer structure and sublayer thickness between *in vivo* images, and *ex vivo* images have been achieved, especially for the small intestine tissue. Ring down artifacts caused by the capsule shell can reduce the visibility of the mucosa layer, while the lumen tissue compresses against the capsule. This may indicate that careful design of the capsule shell will be one of the challenges to be overcome for further development of ultrasound capsule endoscopes.

ACKNOWLEDGEMENTS

This work was supported by UK Engineering and Physical Sciences Research Council Grant entitled *Sonopill* (EP/K034537/1), National Science Foundation Grants of China (11874382, 11804357, 11534013, and 11574342), Natural Science Foundation of Guangdong Province (2015A030306018, 2014B030301013 and 2014A030312006), Shenzhen Research Grant (GJHZ20180420180920529, JCYJ20170817171836611, JCYJ20170413164936017, and ZDSYS201802061806314), Shenzhen Double Chain Project [2018]256, CAS research projects (QYZDB-SSW-JSC018 and YJKYYQ20170065) and Guangdong Special Support Program.

REFERENCES

Arneson M, Bandy W, Shanks W. Ultrasound Scanning Capsule Endoscope (USCE). 2014.

Basar MR, Malek F, Juni KM, Idris MS, Saleh MIM. Ingestible Wireless Capsule Technology: A Review of Development and Future Indication. Int J Antennas Propag 2012;2012:1–14.

Ciuti G, Caliò R, Camboni D, Neri L, Bianchi F, Arezzo A, Koulaouzidis A, Schostek S, Stoyanov D, Oddo CM, Magnani B, Menciassi A, Morino M, Schurr MO, Dario P. Frontiers of robotic endoscopic capsules: a review. J Micro-Bio Robot Journal of Micro-Bio Robotics, 2016;11:1–18.

Correia J. Final Report Summary - TROY (Endoscope Capsule using Ultrasound Technology). 2009.

Cox BF, Stewart F, Lay H, Cummins GC, Newton IP, Desmulliez MPY, Steele RJC, Näthke I, Cochran S. Ultrasound capsule endoscopy: sounding out the future. Ann Transl Med 2017;5:201–201.

Cummins G, Cox BF, Ciuti G, Anbarasan T, Desmulliez MPY, Cochran S, Steele R, Plevris JN, Koulaouzidis A. Gastrointestinal diagnosis using non-white light imaging capsule endoscopy. Nat Rev Gastroenterol Hepatol 2019;16:429–447.

Dimagno E, Regan P, Wilson D, Buxton J, Hattery R, Suarez J, Green P. Ultrasonic Endoscope. Lancet 1980;315:629–631.

Gora MJ, Sauk JS, Carruth RW, Gallagher KA, Suter MJ, Nishioka NS, Kava LE, Rosenberg M, Bouma BE, Tearney GJ. Tethered capsule endomicroscopy enables less invasive imaging of gastrointestinal tract microstructure. Nat Med Nature Publishing Group, 2013;19:238–40.

Hamilton MJ. The valuable role of endoscopy in inflammatory bowel disease. Diagn Ther Endosc 2012;2012:467979.

Iddan G. Ultrasonic capsule with rotatable reflector. 2010.

Iddan G, Meron G, Glukhovsky A, Swain P. Wireless capsule endoscopy. Nature 2000;405:417–417.

Kararli TT. Comparison of the gastrointestinal anatomy, physiology, and biochemistry of humans and commonly used laboratory animals. Biopharm Drug Dispos 1995;16:351–80.

Lay HS, Cox BF, Seetohul V, Demore CEM, Cochran S. Design and Simulation of a Ring-Shaped Linear Array for Microultrasound Capsule Endoscopy. IEEE Trans Ultrason Ferroelectr Freq Control 2018;3010:1–1.

Lay HS, Cummins G, Cox BF, Qiu Y, Turcanu MV, McPhillips R, Connor C, Gregson R, Clutton E, Desmulliez MPY, Cochran S. <italic>In-Vivo</italic> Evaluation of Microultrasound and Thermometric Capsule Endoscopes. IEEE Trans Biomed Eng 2019;66:632–639.

Lee JH, Traverso G, Schoellhammer CM, Blankschtein D, Langer R, Thomenius KE, Boning DS, Anthony BW. Towards wireless capsule endoscopic ultrasound (WCEU). 2014 IEEE Int Ultrason Symp IEEE, 2014 [cited 2014 Oct 28]. pp. 734–737.

McNally PR. Endoscopic Ultrasound. In: McNally PR, ed. GI/Liver Secrets Fourth. Elsevier Health Sciences, 2010. pp. 537–544.

Memon F, Touma G, Wang J, Baltsavias S, Moini A, Chang C, Rasmussen MF, Nikoozadeh A, Choe JW, Olcott E, Jeffrey RB, Arbabian A, Khuri-Yakub BT. Capsule ultrasound device: Further developments. 2016 IEEE Int Ultrason Symp IEEE, 2016. pp. 1–4.

Memon F, Touma G, Wang J, Baltsavias S, Moini A, Chang C, Rasmussen MF, Nikoozadeh A, Jung Woo Choe, Arbabian A, Jeffrey RB, Olcott E, Khuri-Yakub BT. Capsule ultrasound device. 2015 IEEE Int Ultrason Symp IEEE, 2015. pp. 1–4.

Moglia A, Menciassi A, Dario P, Cuschieri A. Capsule endoscopy: progress update and challenges ahead. Nat Rev Gastroenterol Hepatol 2009;6:353–361.

Panes J, Bouhnik Y, Reinisch W, Stoker J, Taylor SA, Baumgart DC, Danese S, Halligan S, Marincek B, Matos C, Peyrin-Biroulet L, Rimola J, Rogler G, van Assche G, Ardizzone S, Ba-Ssalamah A, Bali MA, Bellini D, Biancone L, Castiglione F, Ehehalt R, Grassi R, Kucharzik T, Maccioni F, Maconi G, Magro F, Martín-Comín J, Morana G, Pendsé D, Sebastian S, Signore A, Tolan D, Tielbeek JA, Weishaupt D, Wiarda B, Laghi A. Imaging techniques for assessment of inflammatory bowel disease: joint ECCO and ESGAR evidence-based consensus guidelines. J Crohns Colitis 2013;7:556–85.

Saar LI. Lymph Nodes of the Head, Neck and Shoulder Region of Swine. Iowa State Univ Vet 1962;25:120–134.

Schembre D, Ayub K, Jiranek G. High-frequency mini-probe ultrasound: the Rodney Dangerfield of endoscopy? J Clin Gastroenterol 2005;39:555–6.

Seibel EJ, Carroll RE, Dominitz JA, Johnston RS, Melville CD, Lee CM, Seitz SM, Kimmey MB. Tethered capsule endoscopy, a low-cost and high-performance alternative technology for the screening of esophageal cancer and Barrett's esophagus. IEEE Trans Biomed Eng 2008;55:1032–1042.

Stewart F, Qiu Y, Lay H, Newton I, Cox B, Al-Rawhani M, Beeley J, Liu Y, Huang Z, Cumming D, Näthke I, Cochran S. Acoustic Sensing and Ultrasonic Drug Delivery in Multimodal Theranostic Capsule Endoscopy. Sensors 2017;17:1553.

Swindle MM, Makin A, Herron AJ, Clubb FJ, Frazier KS. Swine as Models in Biomedical Research and Toxicology Testing. Vet Pathol 2012;49:344–356.

Valdastri P, Simi M, Webster RJ. Advanced Technologies for Gastrointestinal Endoscopy. Annu Rev Biomed Eng 2012;14:397–429.

Wang A, Banerjee S, Barth BA, Bhat YM, Chauhan S, Gottlieb KT, Konda V, Maple JT, Murad F, Pfau PR, Pleskow DK, Siddiqui UD, Tokar JL, Rodriguez SA. Wireless capsule endoscopy. Gastrointest Endosc 2013;78:805–815.

Wang J, Memon F, Touma G, Baltsavias S, Jang JH, Chang C, Rasmussen MF, Olcott E, Jeffrey RB, Arbabian A, Khuri-Yakub BT. Capsule ultrasound device: Characterization and testing results. 2017 IEEE Int Ultrason Symp IEEE, 2017a. pp. 1–4.

Wang X, Seetohul V, Chen R, Zhang Z, Qian M, Shi Z, Yang G, Mu P, Wang C, Huang Z, Zhou Q, Zheng H, Cochran S, Qiu W. Development of a Mechanical Scanning Device With High-Frequency Ultrasound Transducer for Ultrasonic Capsule Endoscopy. IEEE Trans Med Imaging 2017b;36:1922–1929.

Yu M, Li Y, Ma T, Shung KK, Zhou Q. Intravascular Ultrasound Imaging with Virtual Source Synthetic Aperture Focusing and Coherence Factor Weighting. IEEE Trans Med Imaging IEEE, 2017;36:2171–2178.

Ziegler A, Gonzalez L, Blikslager A. Large Animal Models: The Key to Translational Discovery in Digestive Disease Research. Cell Mol Gastroenterol Hepatol 2016;2:716–724.

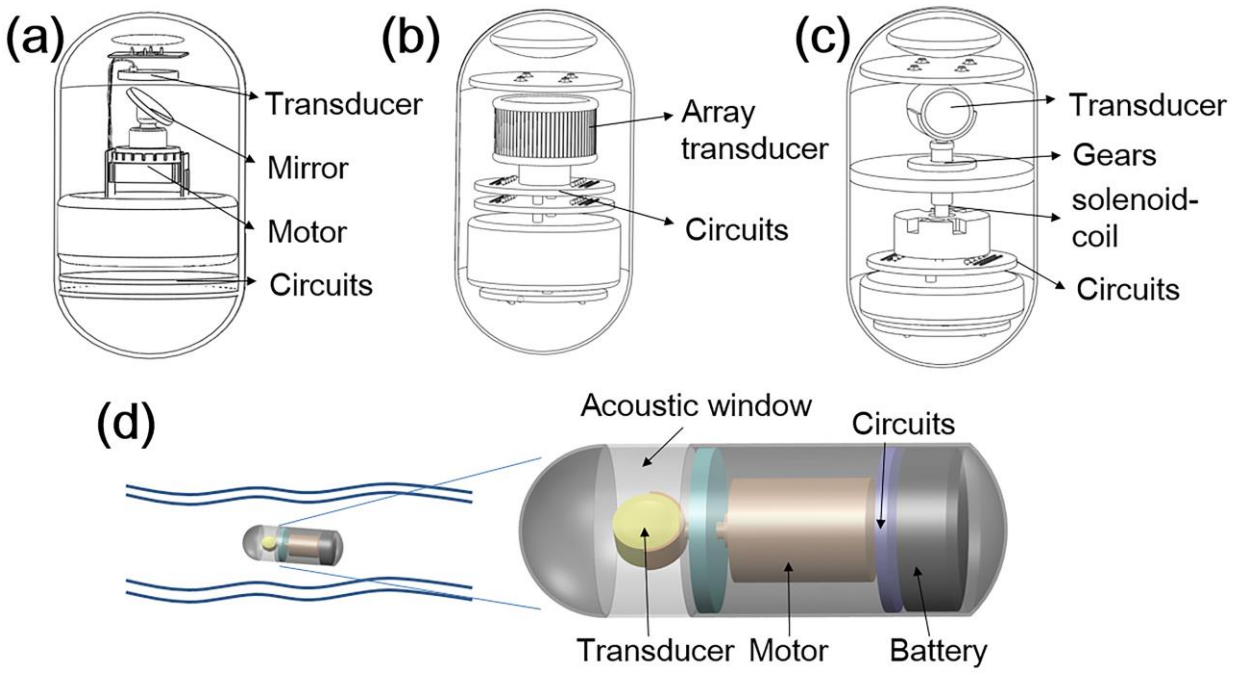

Figure 1. The schemes towards for ultrasound capsule. (a) A mirror was employed for ultrasound reflection; (b) Circular array transducer-based scheme; (c) A solenoid coil was used to rotate the transducer through gears; (d) A micro-motor was employed to rotate the transducer back and forth for circular imaging.

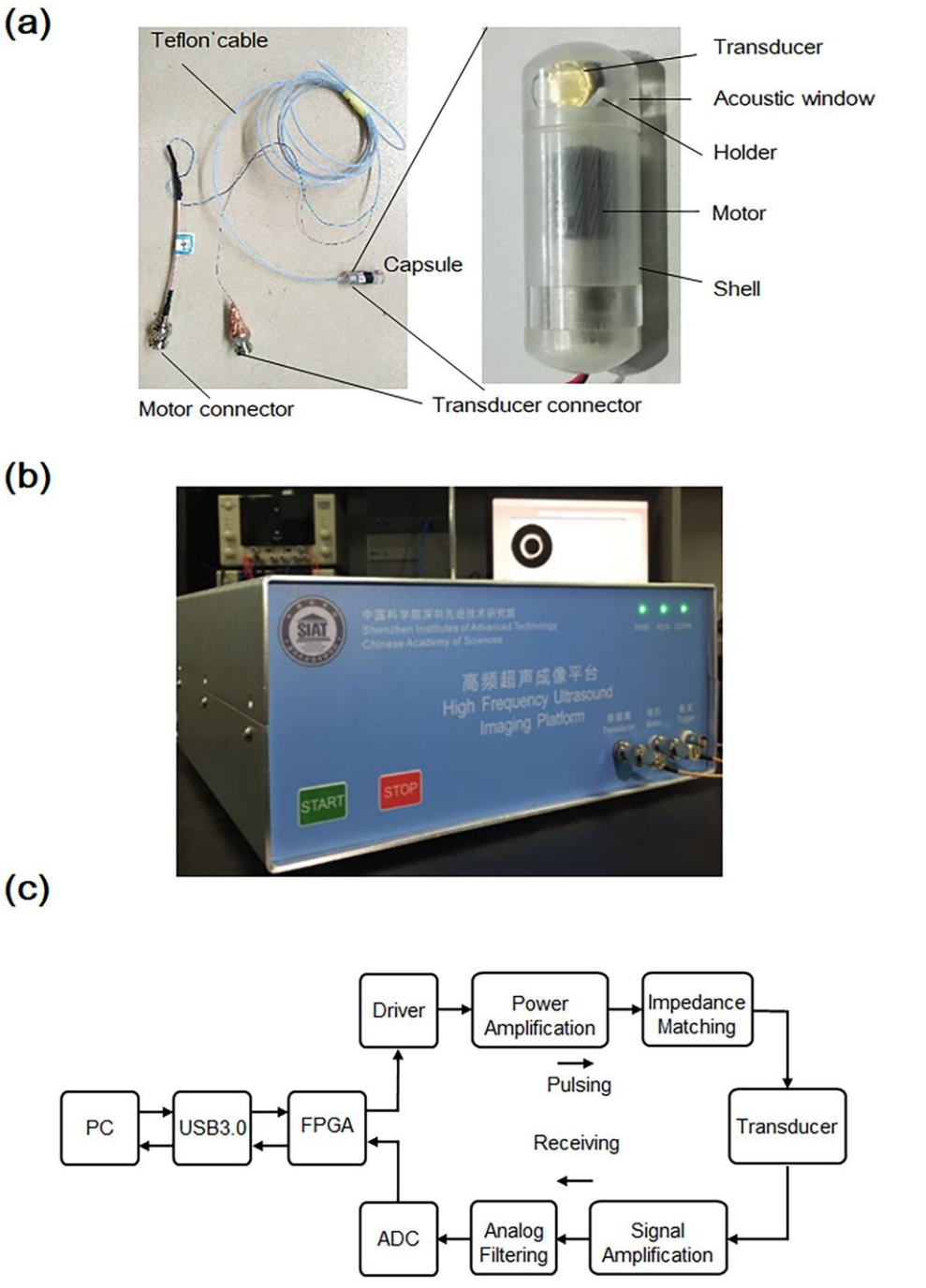

Figure 2. (a) Tethered μUSCE device, (b) high-frequency ultrasound imaging and motor control system, (c) a process diagram of the ultrasound imaging process.

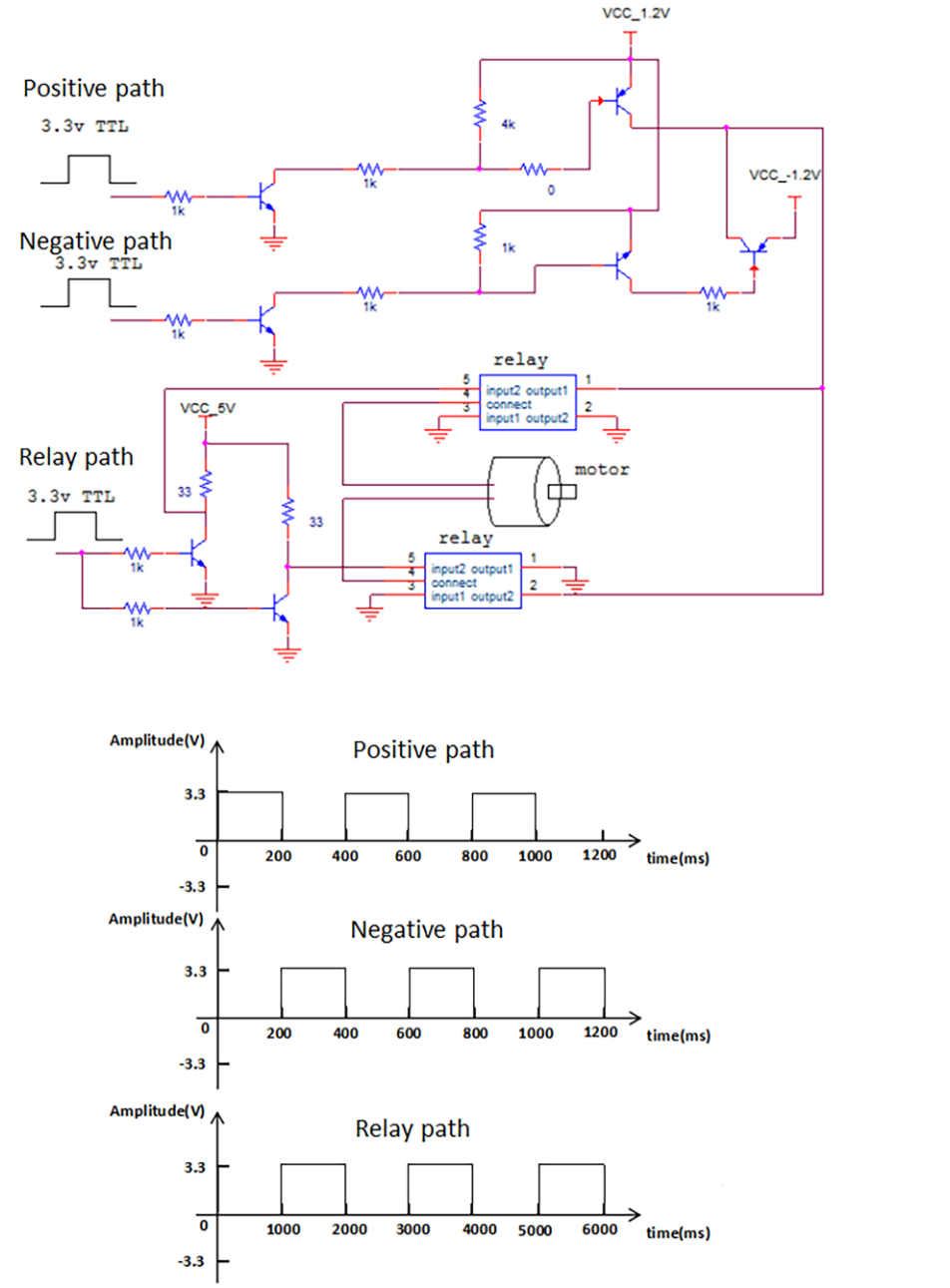

Figure 3. Micromotor control circuit diagram with input time sequences.

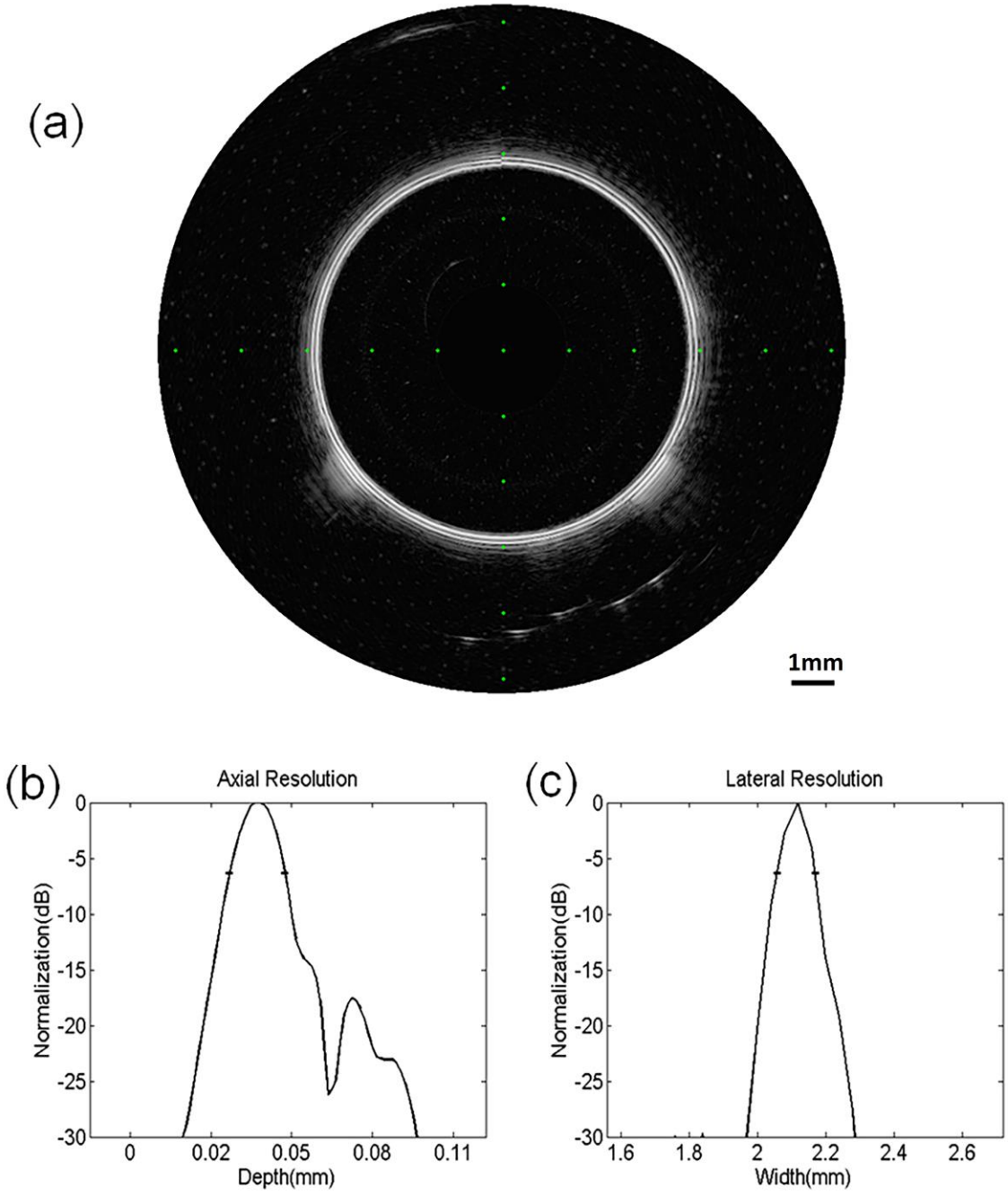

Figure 4. (a) An ultrasound B-scan image of the wire phantom, with (b) axial and (c) lateral resolutions.

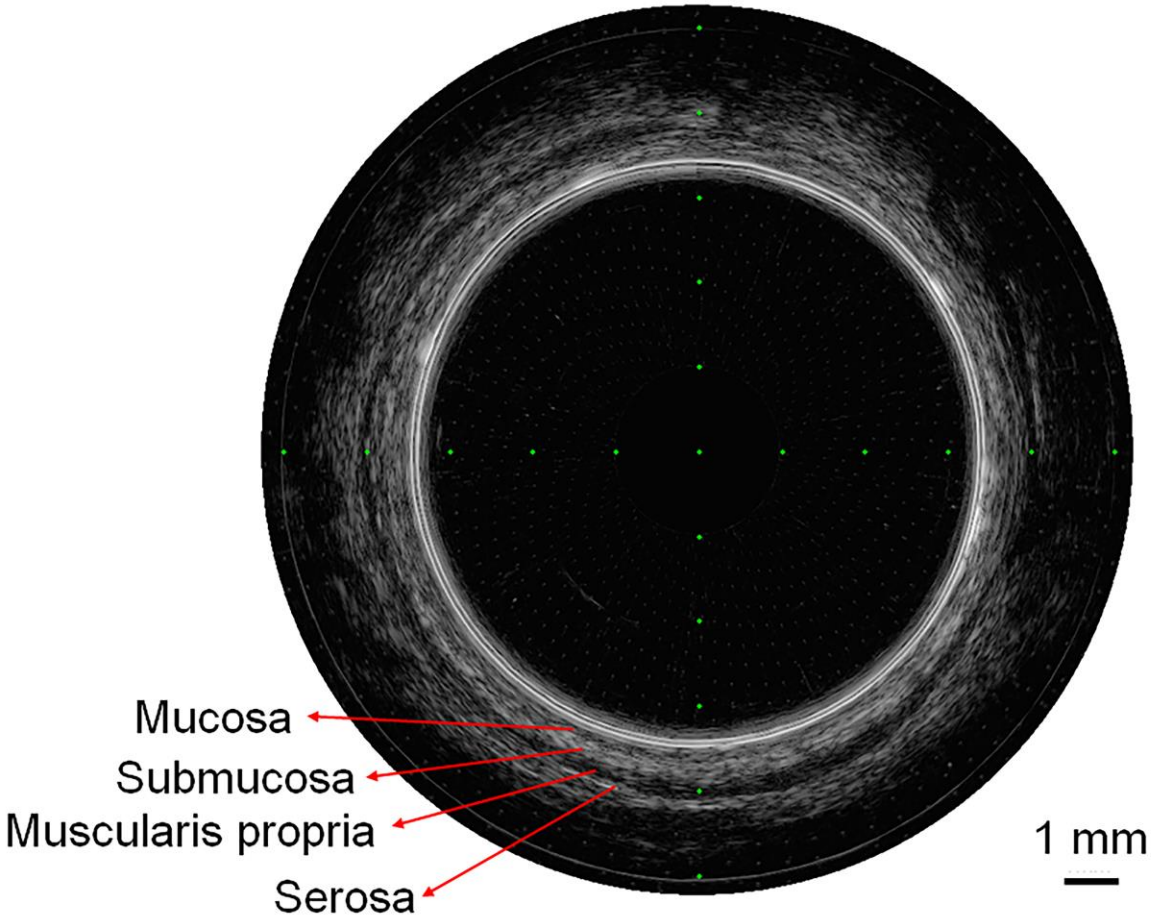

Figure 5. A post-processed cross-sectional ultrasound B-scan transmural image of a pig small intestine. Cardinal histological layers have been labelled from the superficial luminal layer (i.e. Mucosa) to the deeper layer (Serosa).

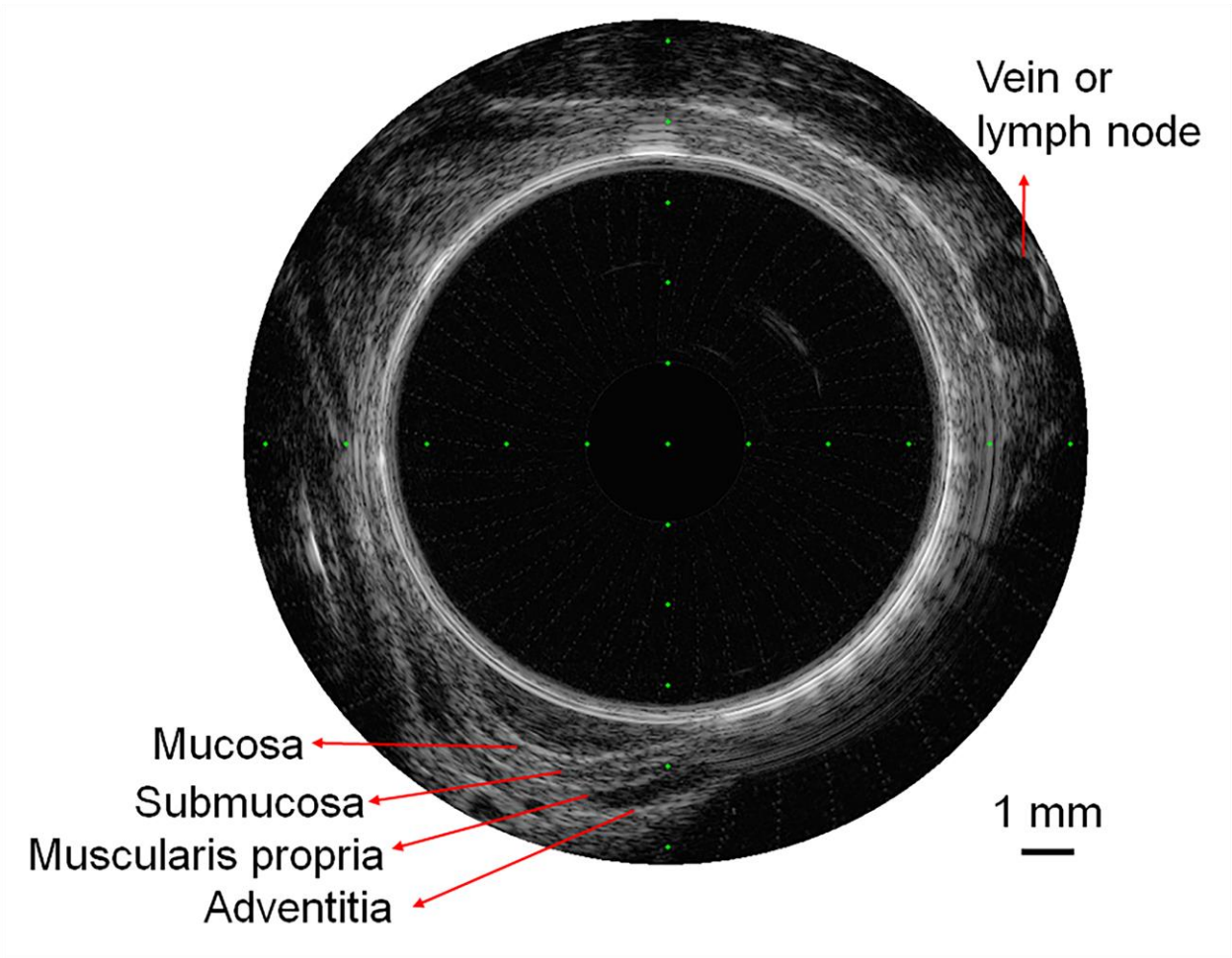

Figure 6. A post-processed cross-sectional ultrasound B-scan transmural image of a pig oesophagus. Cardinal histological layers have been labelled from the superficial luminal layer (i.e. Mucosa) to the deeper layer (Adventitia).